JOURNAL OF AGRICULTURAL AND FOOD CHEMISTRY

pubs.acs.org/JAFC Article

Genome Mining of *Chromobacterium* Genus Reveals a Class of Nonribosomal Lipopeptides with Potent Antifungal Activity

Qinghong Meng, Yutian Guan, Jinghai Wang, Xingyan Wang, Xiangmei Ren, Haiyan Sui, Bin Wei,* and Xiaoying Bian*

Cite This: https://doi.org/10.1021/acs.jafc.5c04892 Read Online

ACCESS | Metrics & More | Article Recommendations | Supporting Information

ABSTRACT: Bacterial genomes encode numerous cryptic biosynthetic gene clusters (BGCs) that represent an untapped potential source of drugs or biopesticides. However, the limited analysis of BGCs in a specific genus has limited the discovery of their natural products through genome mining. Herein, we report the systematic analysis of the biosynthetic potential of 136 genomes of the *Chromobacterium* genus. A total of 1713 BGCs were identified and grouped into 190 gene cluster families (GCFs). However, only eight BGCs from seven GCFs have been functionally characterized, highlighting the vast underexplored potential of the genus for the production of novel natural products. Guided by this analysis, we investigated a cryptic BGC of GCF9 featuring a glycosyltransferase and a nonribosomal peptide synthetase (NRPS) with a starter condensation domain, leading to the identification of a class of glycolipopeptides chromorhipeptins from *Chromobacterium rhizoryzae*. Chromorhipeptins A and B demonstrated broad-spectrum antifungal activity against several plant pathogenic fungi, including *Valsa mali*, with minimum inhibitory concentrations (MICs) at 0.04 and 0.16 μM, respectively, outperforming the fungicide carbendazim (MIC = 0.78 μM). These findings revealed the biosynthetic potential of *Chromobacterium* and underscored the power of genome mining to unlock cryptic bacterial natural products for crop protection against plant pathogenic fungi.

KEYWORDS: *natural product, genome mining, antifungal activity, nonribosomal lipopeptides, Chromobacterium*

INTRODUCTION

Bacteria are a vital source of bioactive natural products for the development of therapeutic agents and ecofriendly biopesticides.[1−3] Global analysis of bacterial genomes show that only 3% of the natural products potentially encoded in bacterial genomes have been experimentally characterized,[4,5] leaving many biosynthetic gene clusters (BGCs) in bacteria to be explored for novel bioactive natural products.[5] Genome mining has accelerated the discovery of new natural products through bioinformatic-guided prioritization of cryptic BGCs.[6−8] However, the lack of detailed analysis of the BGCs within specific genera, such as *Chromobacterium* spp., has limited the further discovery of its natural products via genome mining.

The genus *Chromobacterium*, classified within the family *Chromobacteriaceae*, order *Neisseriales*, class *β-Proteobacteria*, is Gram-negative bacteria with remarkable secondary metabolic versatility, including alkaloids, peptides and polyketides.[9−14] These bacteria are predominantly distributed in tropical and subtropical aquatic and soil ecosystems, with certain species colonizing continental low-temperature regions and even the human gut.[15,16] *Chromobacterium* spp. produce pharmaceutically significant natural products (NPs), including the FDA-approved anticancer agent romidepsin (FK228),[9] potent Gq protein inhibitor FR900359,[10] and antibacterial agent violacein.[11] In addition, *Chromobacterium* spp. have been used in agriculture for pest control; for example, *Chromobacterium subtsugae* strain PRAA4-1 is the active ingredient of the bioinsecticide Grandevo.[17] However, NPs research in this genus mainly focused on the model species *C. violaceum*, and most compounds were discovered before the 2000s, except for the genome mining of the lipopeptides valhidepsins from *C. vaccinii*,[18,19] This suggests that its biosynthetic potential remains largely unexplored. Therefore, an *in silico* systematic analysis of BGCs in *Chromobacterium* would facilitate the evaluation of the biosynthetic potential and the discovery of bioactive compounds from this genus through genome mining.

Nonribosomal peptide synthetases (NRPSs) are the most widespread natural product BGCs in bacterial genomes,[20] and these products nonribosomal peptides (NRPs) have rich structural and bioactive diversity.[21] NRPSs usually comprise several modules, each module generally containing adenylation (A) domain, condensation (C) domain, and the peptidyl carrier protein (PCP),[22] which is responsible for amino acid activation and peptide bond formation.[23] The selectivity of NRPS A domains combined with the catalytic domain organization that generally follows the collinearity principle enables the predict of amino acid building blocks and the putative peptide structure.[23,24] The diversity of NRPs generally originates from the different substrates of the A domains, multiple types of C domains, the presence of optional domains such as epimerization (E) and methylation (MT) domains,

Received: April 17, 2025
Revised: August 8, 2025
Accepted: August 11, 2025

and postassembly modifications such as glycosylation catalyzed by glycosyltransferases.[25,26] In general, glycosylation increases the diversity of peptides and broadens the range of functionality.[27] Some NRPs have a fatty acyl chain at their N-terminal to form the nonribosomal lipopeptide (NRLP), which is introduced by a starter condensation (Cs) domain or fatty acyl ligase at the initiation of NRPS, and the fatty acyl chains of lipopeptides show significant effects on their biological activities.[28−31] NRLPs play critical pharmaceutical roles as antibiotics (e.g., daptomycin and polymyxin), while also serve as principal antifungal substances of biocontrol bacteria, such as surfactin, fengycin, and iturin from *Bacillus* spp. and syringomycin, viscosin, and tolaasin from *Pseudomonas* spp.[32−34]

Because lipidation and glycosylation enhance the membrane targeting ability of antimicrobial compounds and pharmacokinetic properties, they are the two common modification approaches to increase peptide efficacy.[35] NRLP BGCs containing glycosyltransferase genes usually produce glycosylated NRLPs, also known as glycolipopeptides, representing an intriguing class of peptides with lipidation and glycosylation modifications, e.g., the antifungal occidiofungins from *Burkholderia* spp.[36] and the antifungal and cytotoxic hassallidins produced by cyanobacteria.[37] Thus, genome mining of potential glycolipopeptide BGCs facilitates the discovery of bioactive natural products.

In the present study, we first systemically analyze the BGCs and gene cluster families (GCFs) in the *Chromobacterium* genus, revealing its large biosynthetic potential. Among these GCFs, GCG9 harboring a Cs domain-contained NRPS together with a glycosyltransferase, suggesting its product could be a class of glycolipopeptides. Guided by this analysis, the products of a cryptic NRPS BGC *chr* (belong to GCF9) in *C. rhizoryzae*, chromorhipeptins A−D, was identified by CRISPR/Cas9-mediated gene inactivation, compound purification, and structural elucidation. Chromorhipeptins A and B exhibited potent antifungal activity against plant pathogenic fungi such as *Valsa mali* (apple canker), surpassing the commercial fungicide carbendazim, demonstrating the power of genome mining to discover bioactive natural products for agriculture applications.

MATERIALS AND METHODS

General Experimental Procedures. Optical rotations were obtained on a Rudolph AUTOPOL IV automatic polarimeter and were uncorrected. All NMR spectra were acquired on a Bruker AVNEO 600 MHz NMR spectrometer. HRESIMS data were obtained on a Bruker Impact HD microTOF Q III mass spectrometer (Bruker Daltonics, Bremen, Germany) operating in positive-ion mode with direct infusion. HPLC-MS was operated using a Thermo Scientific Dionex Ultimate 3000 system equipped with a Thermo Scientific Acclaim C_{18} column (2.1 × 100 mm, 2.2 μm). Column chromatography was performed using reversed phase C18 gel (YMC). Semipreparative reversed-phase HPLC was performed on an Agilent 1260 Infinity II (Agilent Technologies) or a Shimadzu Essentia LC-16 liquid chromatography system with an ODS column (Agilent ZORBAX Eclipse XDB-C18, 9.4 × 250 mm, 5 μm, 2.5 mL/min).

Whole-Genome Sequencing and Analysis. The whole-genome sequencing of *C. rhizoryzae* was completed with the Illumina and Nanopore platforms from Wuhan Benagen Technology Co., Ltd. The Unicycler[38] (Version 0.5.0) sequence assembly system was used to assemble the genome.

Global Genome Mining of BGCs in *Chromobacterium* Genomes. *Genome Collection and Phylogenetic Analysis.* A total of 131 *Chromobacterium* genomes were retrieved from the National Center for Biotechnology Information (NCBI; https://www.ncbi.nlm.nih.gov/)[39] (data updated to July 2024) and supplemented with five additional genomes from our laboratory collection. Genomic metadata, including accession numbers, genome sizes, and assembly types, were downloaded via the NCBI FTP server. Assembly quality of all 136 genomes was assessed using CheckM2[40] (v1.0.2) to evaluate completeness and contamination rates. Phylogenetic reconstruction was performed with UBCG[41] (v3.0) based on their conserved bacterial marker genes, and the resulting tree was visualized and annotated using iTOL[42] (Interactive Tree of Life).

Diversity and Novelty Analysis of Biosynthetic Gene Clusters (BGCs). All genomes were processed using the command-line version of antiSMASH[43] (v7.1.0) with default parameters for BGC prediction. A custom Python toolkit (https://github.com/BioGavin/astool) was employed to extract the number and class of BGCs, along with relevant architecture information, from the antiSMASH outputs. To assess the diversity and novelty of the predicted BGCs, all BGCs were compared to those in the Minimum Information about a Biosynthetic Gene Cluster (MIBiG) database[44] (v4.0) and all previously characterized gene clusters from this genus using biosynthetic gene similarity clustering and prospecting engine (BiG-SCAPE)[45] (v2.0) with a similarity threshold of 0.3. Gene cluster networks were visualized and annotated using Cytoscape[46] (v3.10.0). Clinker[47] was utilized to align and visualize representative BGCs from an NRPS gene cluster family containing a starter condensation (Cs) and uridine diphosphate glycosyltransferase. Fasttree[48] was utilized to align the C domains of the *chr* BGC. The phylogenetical tree was visualized and annotated using iTOL.

Microorganism and Culturing Conditions. The *Chromobacterium rhizoryzae* strain MCCC 1K07697 was isolated from activated sludge that was collected at Xiamen University Sewage Treatment Plant and purchased from the Marine Culture Collection of China (MCCC). For seed culture, a single colony was inoculated into 50 mL of Luria−Bertani (LB) medium (10 g/L tryptone, 5 g/L yeast extract, 10 g/L NaCl) in a 250 mL flask and incubated at 30 °C with shaking (200 rpm) for 24 h. Subsequently, 0.5 mL overnight seed culture was transferred into 50 mL of potato dextrose broth (24 g/L Potato Dextrose Broth) in 250 mL flasks (total: 200 flasks, 10 L medium) at 30 °C, 200 rpm for 3 days. 2% XAD-16 resin was added to adsorb metabolites, followed by methanol extraction (35 mL per flask). The combined extracts were evaporated under reduced pressure. The extract was obtained and analyzed by HPLC-MS according to the report. Empty medium was utilized as acontrol.[49]

Genetic Manipulation. Genetic inactivation of the target genes (Table S1) of *C. rhizoryzae* cluster were used by the CRISPR/Cas9-mediated knockout.[50,51] The CRISPR/Cas9 plasmid was constructed from the sgRNA fragment, pKCcas9dO vector,[52] and 1kb homologous arms at both ends of the desired deletion genomic region via Gibson assembly in the *E. coli* GB05-dir competent cells. The vector fragment was obtained by the double digestion of pKCcas9dO with *Hind*III and *Spe*I. The 1 kb homology arms of *chrA* were amplified by PCR using genomic DNA as the template with primer pairs 7697B4H1-F/R and 7697B4H2-F/R. The sgRNA fragment was generated through two-step PCR amplification using pKCcas9dO as the template with primer pairs gRNA-R-S08/gRNA_target-S08 and gRNA-R-S08/gRNA_target-S08-2. These correct plasmids were verified by restriction digestion. One milliliter of overnight liquid LB culture of *E. coli* ET12567/pUZ8002 was transferred into 1.3 mL fresh LB medium and incubated at 30 °C, 950 rpm for 3 h. Then the cultures were centrifuged at 9600 rpm for 30 s at 25 °C in a centrifuge and the supernatant was discarded as much as possible. The pellets were resuspended in 1 mL precooled ddH_2O. This step was repeated, and the cell pellets were resuspended with 30 μL ddH_2O; 1.5 μg constructed plasmids were added and mixed gently. The plasmid pKCcas9dO-del-dBGC4 was electroporated into *E. coli* ET12567/pUZ8002, and positive transformants were selected using double-antibiotic plates containing kanamycin (Km) and apramycin (Apra). These obtained transformants were subjected to conjugation with *C. rhizoryzae* MCCC 1K07697 on LB agar plates. Leveraging the natural tolerance of the recipient strain MCCC

https://doi.org/10.1021/acs.jafc.5c04892
J. Agric. Food Chem. XXXX, XXX, XXX−XXX

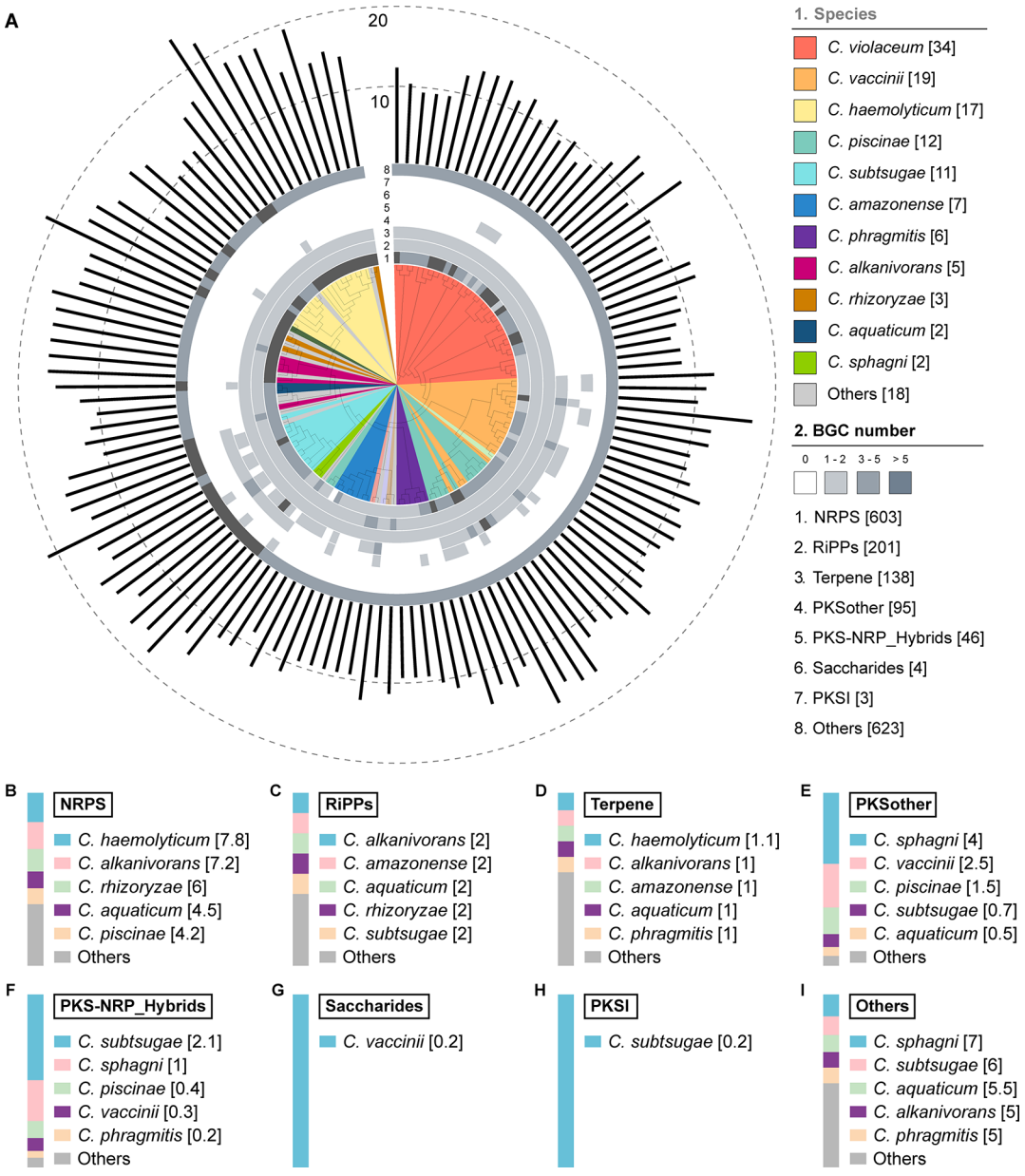

Figure 1. Phylogenetic analysis and distribution of biosynthetic gene clusters (BGCs) in 136 *Chromobacterium* Genomes. (A) The maximum-likelihood phylogenetic tree of 136 *Chromobacterium* genomes is shown, with species classification annotated for 11 clearly defined species; remaining strains are grouped as "Others". Layers 2−9 illustrate the distribution of eight BGC classes: NRPS (nonribosomal peptide synthetases), RiPPs (ribosomally synthesized and post-translationally modified peptides), Terpene, PKSother (other polyketide synthases), PKS-NRP_Hybrids, Saccharides, PKSI (type I polyketide synthases), and Others. Color intensity in each layer corresponds to the number of BGCs per genome for each class. Layer 10 indicates the total BGC count per genome. (B−I) Bar plots depict the mean number of BGCs for each class across 11 *Chromobacterium* species with ≥2 genomes. (B) NRPS, (C) RiPPs, (D) Terpene, (E) PKSother, (F) PKS-NRP_Hybrids, (G) Saccharides, (H) PKSI, (I) Others.

1K07697 to ampicillin (Amp), positive postconjugation colonies were selected using dual-antibiotic plates supplemented with Amp and Apra. Finally, PCR amplification of the target region followed by sequencing was performed to validate the CRISPR/Cas9-mediated gene knockout. This verified colony was fermented, and the crude extract was subjected to LC-MS analysis. The same method was used to knock out genes *chrD* and *chrE*. Strains, plasmids, and PCR primers used in this study are given in Tables S2 and S3.

Purification and Compound Identification. For purification of the chromorhipeptins, a total of 10 L of culture was prepared using PDB medium under conditions similar to those for the small-scale fermentation. After 3 days of incubation, 2% Amberlite XAD-16 resin was added, and the mixture was incubated for another 1 day. The XAD-16 resin was thereafter collected for further extraction by methanol (1L in total). All the organic solvents were combined and dried by the evaporator, resulting to 10 g of crude extracts. The crude extracts were subjected to by ODS silica gel using MeOH-H_2O solvent system (4:6, 5:5, 6:4, 7:3, 8:2, and 1:0 v/v) to obtain six fractions (Fr.1−Fr.6). These fractions were subsequently analyzed by HPLC-MS to check for chromorhipeptins. Fr.5 was purified via semipreparative HPLC (Agilent ZORBAX SB-C18 column, 5 μm, 9.4 × 250 mm) using an isocratic elution of 40% acetonitrile in water (0.1% formic acid) at 2.5 mL/min. Detection wavelengths were set to 210 and 275 nm. Under these conditions, chromorhipeptins A (**1**, 5.0 mg) and B (**2**, 5.0 mg) were isolated. Similarly, Fr.3 yielded

https://doi.org/10.1021/acs.jafc.5c04892
J. Agric. Food Chem. XXXX, XXX, XXX−XXX

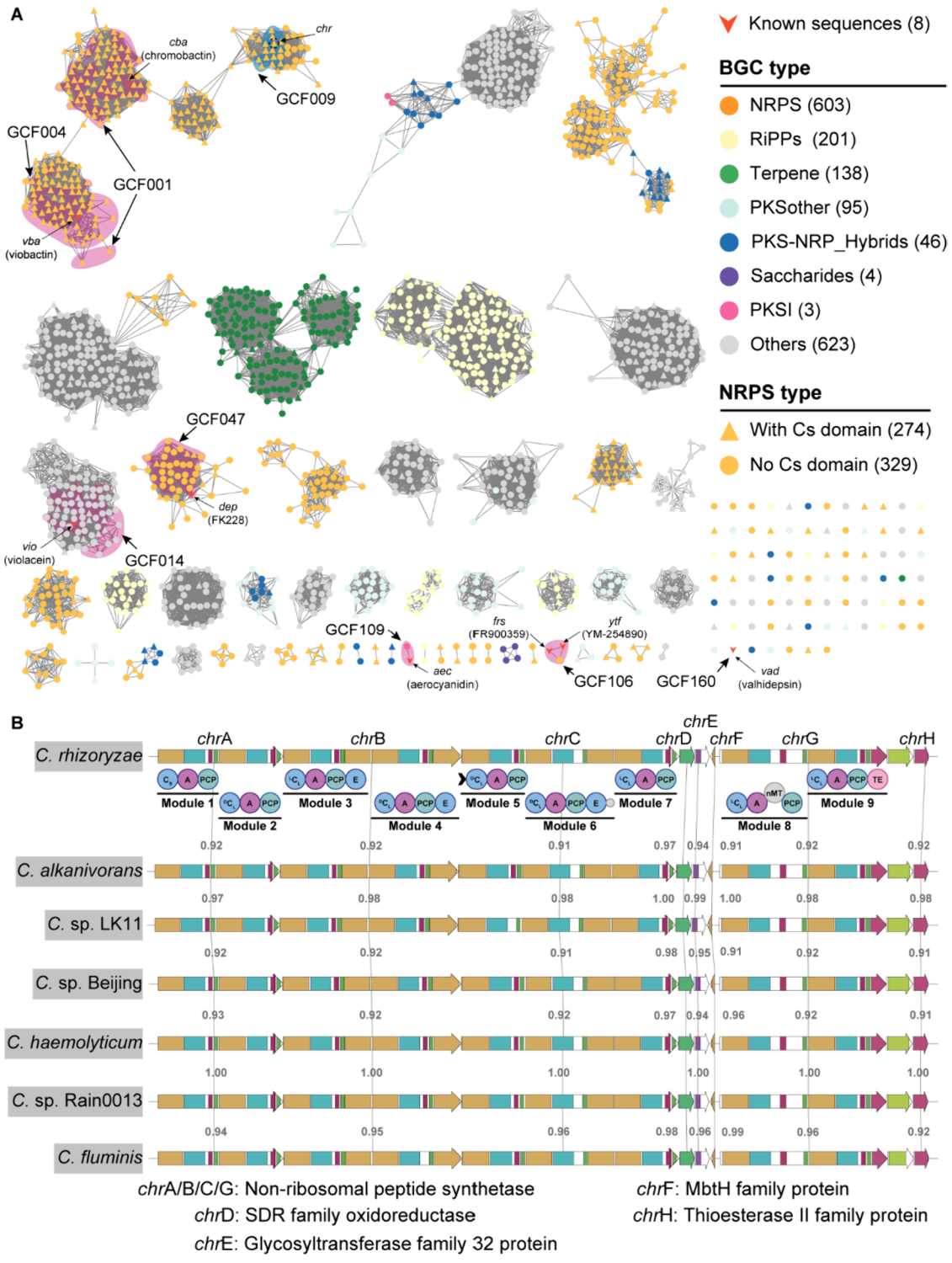

Figure 2. Biosynthetic gene cluster (BGC) similarity network and functional annotation of GCF9. (A) The similarity network of 1713 BGCs from 136 *Chromobacterium* genomes, together with eight characterized gene clusters of this genus clustered into 190 gene cluster families (GCFs) using BIG-SCAPE (v2.0; similarity threshold: 0.3). Nodes represent BGCs, edges denote similarity scores of ≥0.3, and node colors correspond to distinct GCFs. (B) Annotation and comparative analysis of representative BGCs within GCF9, which contain a starter condensation domain and a uridine diphosphate glycosyltransferase.

chromorhipeptins C (**3**, 7.0 mg) and D (**4**, 7.0 mg) under identical chromatographic parameters.

*Chromorhipeptin A (**1**).* White amorphous powder; $[\alpha]^{20}_{D}$ −17.5 (*c* 0.1, MeOH); for ^{1}H and ^{13}C NMR spectroscopic data, see Table S4; HR-ESI-MS *m*/*z* 1195.6363 $[M + H]^+$ (calcd for $C_{57}H_{86}N_{12}O_{16}$, 1195.6358, Δppm = −0.4).

*Chromorhipeptin B (**2**).* White amorphous powder; $[\alpha]^{20}_{D}$ −12.2 (*c* 0.1, MeOH); for ^{1}H and ^{13}C NMR spectroscopic data, see Table S4; HR-ESI-MS *m*/*z* 1357.6815 $[M + H]^+$ (calcd for $C_{63}H_{96}N_{12}O_{21}$, 1357.6886, Δppm = 5.2).

*Chromorhipeptin C (**3**).* White amorphous powder; $[\alpha]^{20}_{D}$ −26.0 (*c* 0.1, MeOH); for ^{1}H and ^{13}C NMR spectroscopic data, see Table

https://doi.org/10.1021/acs.jafc.5c04892
J. Agric. Food Chem. XXXX, XXX, XXX−XXX

S5; HR-ESI-MS m/z 1213.6394 $[M + H]^+$ (calcd for $C_{57}H_{88}N_{12}O_{17}$, 1213.6463, Δppm = 5.7).

*Chromorhipeptin D (**4**).* White amorphous powder; $[\alpha]^{20}{}_D$ −4.07 (c 0.1, MeOH); for ^1H and ^{13}C NMR spectroscopic data, see Table S5; HR-ESI-MS m/z 1375.6920 $[M + H]^+$ (calcd for $C_{63}H_{98}N_{12}O_{22}$, 1375.6991, Δppm = 5.5).

Marfey's Analysis of the Amino Acid Configuration. Absolute configurations of amino acids were determined by Marfey's analysis.[53] Approximately 1 mg of compounds **1**−**4** was hydrolyzed in 6 M HCl (0.5 mL) at 95 °C overnight. Hydrolysates were dried by nitrogen, redissolved in 200 μL of H_2O, and derivatized with 1-fluoro-2,4-dinitrophenyl-5-L-alanine amide (L-FDAA; Sigma-Aldrich) in 1 M $NaHCO_3$ (40 μL) at 40 °C for 1 h. To quench the reaction, 10 μL of 2 M HCl was added. The mixtures were dried under the N_2 gas stream and 200 μL MeOH were added to redissolve the derived residues. Ultimately, the resulting solution was filtered through a small 2.5 μm filter and analyzed by LC-MS with a linear gradient of ACN and 0.1% aqueous FA with different elution conditions (0−3 min, 5% ACN; 3−18 min, 5−95% ACN; 18−22 min, 95% ACN; 22.1 min, 5% ACN; and 22.1−25 min, 5% ACN) at a flow rate of 0.3 mL/min and UV detection at 330 nm. Amino acid standards were derivatized with L-FDAA in a similar manner. Each chromatographic peak was identified by comparing its retention times and mass-to-charge ratios (m/z) for the L-FDAA derivatives of the L- and D-amino acid standards.

Antifungal Screening and Determination of the Minimum Inhibitory Concentration (MIC). The antifungal activity screening of compounds **1**−**4** was tested at a final concentration of 100 μM using the broth dilution method in 96-well sterile culture plates. The microdilution method was used for estimation of the minimum inhibitory concentration (MIC) of chromorhipeptins according to the Clinical Laboratory Standards Institute standard.[54] Serial dilutions of chromorhipeptins A−D (0.05−50.00 μM) were prepared in PDB medium in 96-well plates. Amphotericin B (0.02−25.00 μM) and carbendazim (0.02−25 μM) were included as positive controls. Fungal suspensions (100 μL, 5×10^5 CFU/mL) were added to each well, and plates were incubated at 27 °C for 48 h. Growth inhibition was quantified by measuring the optical density at 600 nm (OD_{600}). The MIC value was defined as the lowest concentration of a test compound that resulted in a culture with a density consistent with 100% inhibition and no detectable growth, as observed by microscopy when compared to the growth of the untreated control. Each of the fungal pathogens was tested in triplicate.

RESULTS

Bioinformatics Analysis of the Biosynthetic Potential of *Chromobacterium* Genus. To accurately evaluate the biosynthetic potential of the *Chromobacterium* genus, we collected all high-quality *Chromobacterium* genome data from a publicly accessible database and generated whole-genome sequences for strains isolated by our group. The most comprehensive and high-quality *Chromobacterium* genome data set to date comprises 136 genomes, covering all 16 species. Among these genomes, 98.53% (134/136) exhibited >98% completeness, 99.26% (135/136) showed <5% contamination, and GC content ranged from 61% to 66% (Table S6). All the 136 genomes yield a total of 1713 BGCs, resulting in an average of 12.6 BGCs per *Chromobacterium* genome. Figure 1A presents the phylogenetic tree of these genomes, along with the distribution of their encoded BGCs. A considerable variation in the number of BGCs can be observed across genomes, ranging from 7 to 24. Among the 16 species analyzed, *C. subtsugae* exhibited the highest average number of BGCs at 15.9, followed by *C. hemolyticum* and *C. sphagni*, with averages of 15.6 and 15.5, respectively. The top three dominant classes of BGCs in this genus are NRPS (603, 35.2%), RiPPs (202, 11.8%), and Terpene (139, 8.1%), underscoring the genus's vast potential for NRPS-derived metabolite biosynthesis. Figure 1B−I illustrates the relative abundance of eight classes of BGCs across different *Chromobacterium* species. The findings demonstrated that NRPS clusters were particularly enriched in *C. hemolyticum*, *C. alkanivorans*, and *C. rhizoryzae*, with mean counts exceeding 6 NRPS BGCs per genome. In contrast, saccharide-related clusters (four types) and polyketide synthase type I (PKS-I) (two types) clusters were exclusively detected in *C. vaccinii* and *C. subtsugae*, suggesting species specialization in secondary metabolism.

The diversity and novelty of BGCs predicted from *Chromobacterium* were analyzed by comparing sequence similarity between themselves and those in this Minimum Information about a Biosynthetic Gene Cluster (MIBiG) database (v4.0) and all earlier characterized gene clusters from this genus using BiG-SCAPE. The 1713 BGCs, together with eight characterized gene clusters were grouped into 190 GCFs, including 79 singleton GCFs (Table S7). Strikingly, only seven GCFs (GCF1, GCF4, GCF14, GCF47, GCF106, GCF109, and GCF160) contained eight functionally characterized BGCs (chromobacin, viobactin, violacein, FK228, FR900359, YM-254890, aerocyanidiin, and valhidepsins),[55−59] highlighting the exceptional capacity of the genus for novel metabolite biosynthesis (Figure 2A). Among these 603 NRPS gene clusters, 274 (45.4%) contain a Cs domain, suggesting that these BGCs use a Cs mechanism to initiate peptide chain synthesis, as exemplified by BGCencoding viobactin (*vio*, GCF4) and chromobacin (*cba*, GCF1). However, the majority of Cs domains containing GCFs remain uncharacterized, highlighting the substantial potential of *Chromobacterium* for the discovery of novel lipopeptide natural products.

Cryptic *chr* BGC of GCF9. GCG9 harbors an NRPS with a Cs domain and a glycosyltransferase, suggesting that its product could be glycolipopeptides, which attracted our interest. Comparative analysis of core biosynthetic genes across among BGCs of GCF9 revealed high sequence similarity (>90%) in *C. hemolyticum*, *C. alkanivorans*, *C. fluminis*, *C.* sp. LK11, *C.* sp. Rain0013, *C.* sp. Beijing, and the *C. rhizoryzae* MCCC no. 1K07697 from our collection. Therefore, we designated this biosynthetic gene cluster as *chr* BGC for further investigation. The *chr* BGC (GenBank accession number, PV690516) includes four NRPSs (ChrA, ChrB, ChrC, and ChrG) containing nine modules, a glycosyltransferase ChrE, a MbtH-like protein ChrF, an SDR family oxidoreductase ChrD, and a type II thioesterase ChrH (Figure 2B). Phylogenetical analysis of the C domains of *chr* BGC (Figure S1) shows a C_S (ChrA-C1), two C_D (ChrA-C2/ChrC-C6) with condensation and dehydration functions, three $^{L}C_L$ (ChrB-C3/ChrG-C8/ChrG-C9) condensing two L-amino acids, and three $^{D}C_L$ (ChrB-C4/ChrC-C5/ChrC-C7) condensing D-amino acid with L-amino acid.[60] Based on the analysis of A domain specificity, the presence of E domains, an *N*-MT domain, and the different subtypes of C domains alongside the nine modules of the NRPS, the peptide is predicted to sequentially incorporate L-Thr/Dhb (dehydroaminobutyric acid)[1], L-Thr[2], D-Thr[3], D-Tyr[4], L-Thr/Dhb[5], D-Gln[6], Gly[7], *N*-methyl-L-threonine (*N*Me-L-Thr)[8], and L-Leu[9]. This analysis suggests these strains can biosynthesize glycosylated liponanopeptides, showing their potential to expand the biosynthetic repertoire of *Chromobacterium* spp.

Identification of the Products of *chr* BGC. To investigate the products of GCF9, *chr* BGC (BGC4) from *C.*

https://doi.org/10.1021/acs.jafc.5c04892
J. Agric. Food Chem. XXXX, XXX, XXX−XXX

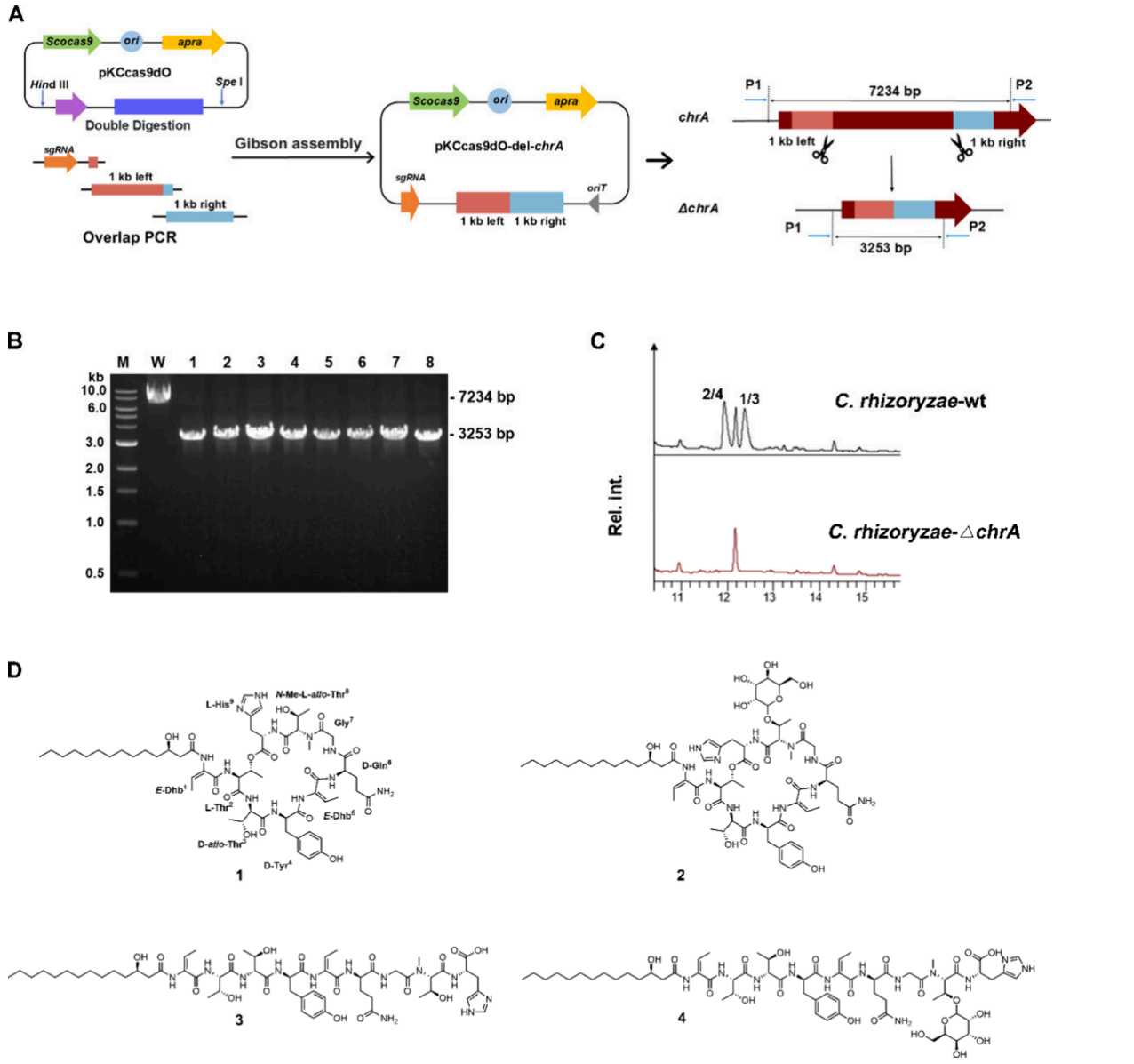

Figure 3. CRISPR-Cas9 mediated gene inactivation enabling the identification of the products of *chr*. (A) CRISPR/Cas9-mediated gene inactivation of the first NRPS gene *chrA*. (B) Verification of knockout mutants by PCR; M, maker; W, wildtype; 1−8, mutant. (C) LC-MS analysis of *C. rhizoryzae* wild type and *chr*-deficient mutant in PDB medium. (D) Structure of chromorhipeptins A−D (**1**−**4**).

rhizoryzae MCCC 1K07697 was selected for product identification. We used CRISPR/Cas9-mediated gene deletion to inactivate the first NRPS gene, *chrA* (Figure 3A). Transformants were screened via polymerase chain reaction (PCR) using flanking primers (Table S2), and a 7.2-kb amplicon was generated in the wild-type (WT) strain, whereas truncated 3.2-kb fragments appeared in the Δ*chrA* mutants. The following sequencing verified the absence of the 3 9 kb fragment in *chrA*, confirming successful inactivation of *chrA* (Figure 3B). Subsequently, we cultured the *C. rhizoryzae* WT strain and the mutant in four distinct media (PDB, LB, NZ, and R2A; Table S8) and analyzed the products through HPLC-MS (Figure S2). Comparative HPLC-MS analysis results show two obvious peaks at the retention time of 11−13 min in the WT, which are absent in the mutant in PDB medium, suggesting that they are products of *chr* BGC, designated as chiromrhipeptions (Figure 3B). Combined with HPLC-MS analysis of the metabolic profiles, the enlarged fermentation of *C. rhizoryzae* wild type were implemented with 10 L PDB medium for 3 days. The crude extracts were then subjected to medium-pressure liquid chromatography and semi-HPLC to obtain four target compounds **1**−**4**, chromorhipeptins A−D (Figure 3C, Figure S3).

Structural Elucidation of Chromorhipeptins. Compound **1** was obtained as a white powder by chromatographic purifications. Its molecular formula was determined as $C_{57}H_{86}N_{12}O_{16}$ (21 degrees of unsaturation) based on the HR-ESI-MS data (*m*/*z* 1195.6363 $[M + H]^+$, calcd. 1195.6358) combined with ^1H and ^{13}C NMR spectroscopic data (Table S4). Combined analysis of ^1H and HSQC spectra of **1** revealed characteristic typical of a peptide, including six α-amino methine proton signals (δ_H 4.49, 4.52, 4.56, 4.58, 4.60, and 4.67), and two α-amino methylene proton signals (δ_H 3.76, 4.00). In addition, six aromatic protons (δ_H 6.53, 6.53, 6.67, 6.67, 7.64, and 7.68), two olefinic methine hydrogens (δ_H 5.60, 5.73), and one singlet *N*-methyl (*N*Me) proton (δ_H 2.41)

https://doi.org/10.1021/acs.jafc.5c04892
J. Agric. Food Chem. XXXX, XXX, XXX−XXX

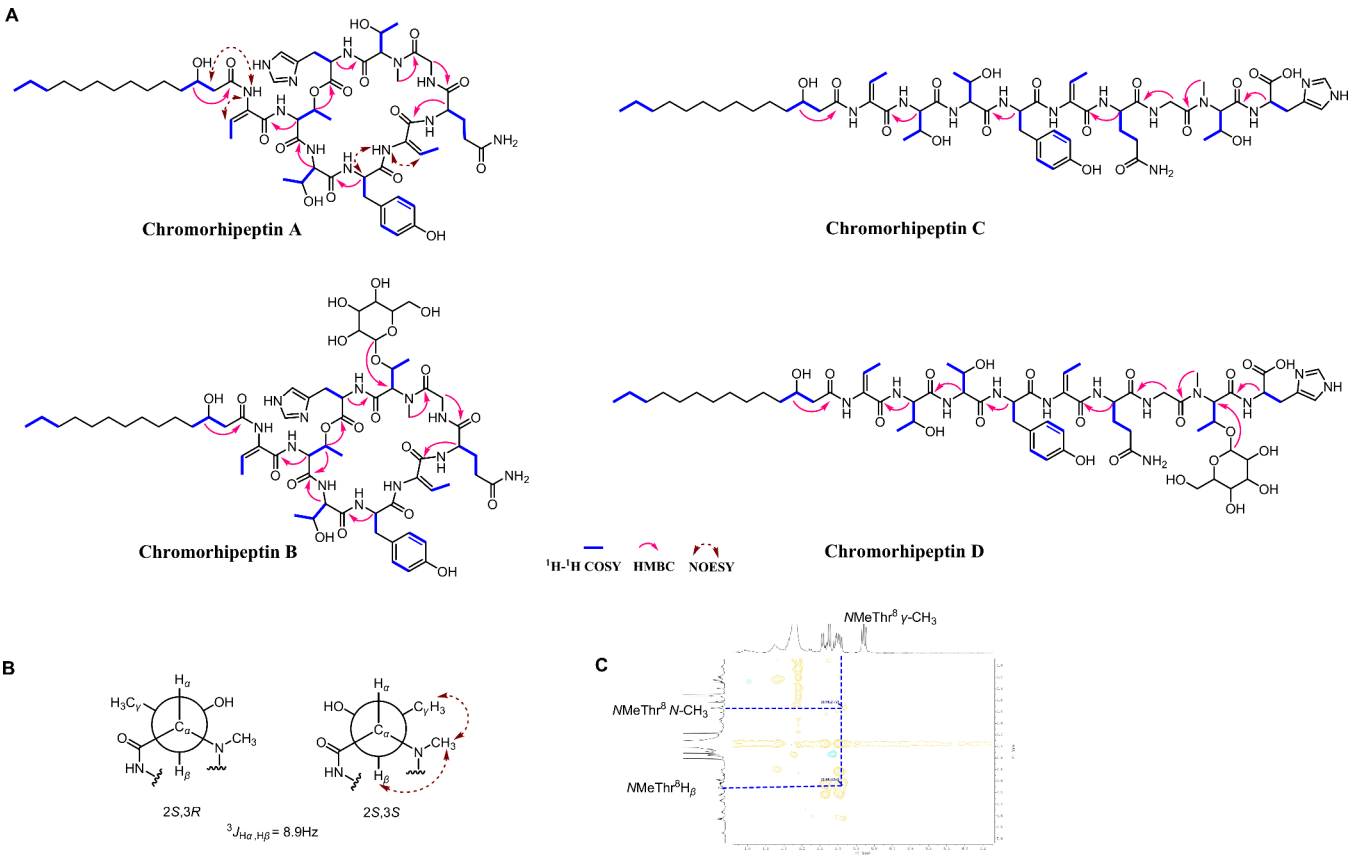

Figure 4. Structural elucidation of chromorhipeptins A–D (**1**–**4**). (A) Key COSY, HMBC, and NOESY correlations were detected. (B) *J*-based configuration analysis of the *N*MeThr residue in **1**. The Newman projection of two possible stereoisomers of the *N*MeThr. (C) Cross-peaks from *N*MeThr γ-CH_3 to adjacent protons in the NOESY spectrum of **1**.

were identified in the structure of **1**. Detailed analysis of the ^{1}H, ^{13}C, DEPT, and HSQC spectra revealed that **1** possessed 11 carbonyl carbon atoms (δ_C 164.4, 166.5, 169.9, 171.1, 171.1, 171.2, 171.7, 171.8, 172.8, 176.0, and 176.2), seven carbon atoms at the α position of the amino acids (δ_C 41.1, 50.9, 51.2, 52.3, 52.4, 55.2, and 55.6), a disubstituted aromatic ring (δ_C 115.2, 115.2, 127.6, 129.8, 129.8, and 155.5), two olefinic methine carbons (δ_C 119.4, 132.4), a heteroaromatic ring (δ_C 129.4, 134.9), and a *N*-methyl group (δ_C 30.3). These account in combination for 20 out of the 21 double-bond equivalents of **1**, thereby suggesting a cyclic structure for **1**.

Combined analysis of the COSY and HMBC NMR data revealed two dehydroaminobutyric acids (Dhb), two Thr, one Tyr, one Gln, one Gly, one *N*MeThr, one His, and one β-hydroxymyristic acid (HMA) to be present in **1**. The COSY correlations revealed 10 discrete spin systems: (1 and 2) H_β(=CH)–CH_3 for Dhb^1 and Dhb^5; (3 and 4) H_α–H_β–CH_3 for Thr^2 and Thr^3; (5) H_α–H_β (aliphatic) and H_2–H_3, H_5–H_6 (aromatic) for Tyr^4; (6) H_α–H_β–H_γ for Gln^6; (7) H_α–H_β (geminal) for Gly^7; (8) H_α–H_β–CH_3 for *N*MeThr^8; (9) H_α–H_β for His^9 residue; and (10) H_α–H_β–H_γ and H_ν–CH_3 for HMA residues. The amino acid sequence in **1** was determined through an extensive analysis of HMBC and NOESY correlations (Figure 4). Four contiguous segments were thereby identified. The first contiguous segment (Dhb^1-Thr^2-Thr^3-Tyr^4) was established by the HMBC correlation from H_α-Thr^2 (δ_H 4.60) to the carbonyl carbon (δ_C 166.5) of Dhb^1, H_α-Thr^3 (δ_H 4.56) to the carbonyl carbon (δ_C 171.1) of Thr^2, and H_α-Tyr^4 (δ_H 4.58) to the carbonyl carbon (δ_C 171.1) of Thr^3. The second contiguous segment (Dhb^5-Gln^6-Gly^7-*N*MeThr^8-His^9) was established via the HMBC correlation from H_α-Gln^6 (δ_H 4.52) to the carbonyl carbon (δ_C 164.4) of Dhb^5, H_α-Gly^7 (δ_H 3.76/4.00) to the carbonyl carbon (δ_C 171.8) of Gln^6, *N*-methyl (*N*Me) protons (δ_H 2.71) of *N*MeThr^8 to the carbonyl carbon (δ_C 171.2) of Gly^7, and H_α-His^9 (δ_H 4.49) to the carbonyl carbon (δ_C 169.4) of *N*MeThr^8. Other contiguous segments of HMA-Dhb^1 and Tyr^4-Dhb^5 were established by the NOESY correlations (Figure 4A) from the amide hydrogen (δ_H 9.55) of Dhb^1 to H_α-HMA (δ_H 2.25) and H_α -Tyr^4 (δ_H 4.58) to the amide hydrogen (δ_H 9.61) of Dhb^5. In addition, the amino acid sequence of **1** was further supported by the observed MS/MS fragment ions (Figure S4) and the bioinformatics analysis. The macrocyclic lipodepsipeptide of compound **1** was established by the HMBC correlation from H_β (δ_H3.58) of Thr^2 to the carbonyl carbon (δ_C 176.2) of His^9 (Figure 4A), confirming the ester bond linkage between them. The planar structure of **1** was deduced as HMA-Dhb^1-cyclo (-Thr^2-Thr^3-Tyr^4-Dhb^5-Gln^6-Gly^7-*N*MeThr^8-His^9-).

Configurations of two Dhb were identified as *E* based on the NOESY correlations (Figure 4A), which showed a correlation from the amino proton (δ_H 9.26, 9.55) to the olefinic proton (δ_H 5.63, 5.73), respectively.[61] The absolute configurations of the amino acids present in **1** were determined as L-Thr^2, D-*allo*-Thr^3, D-Tyr^4, D-Gln^6, and L-His^9 by a modified Marfey's method (Figure S5). Due to the lack of commercially available *N*MeThr, the absolute configuration of *N*-Me-Thr^8 could not be determined by Marfey's method. As *N*MeThr contains the typical vicinal methine protons, the *J*-based configuration

https://doi.org/10.1021/acs.jafc.5c04892
J. Agric. Food Chem. XXXX, XXX, XXX–XXX

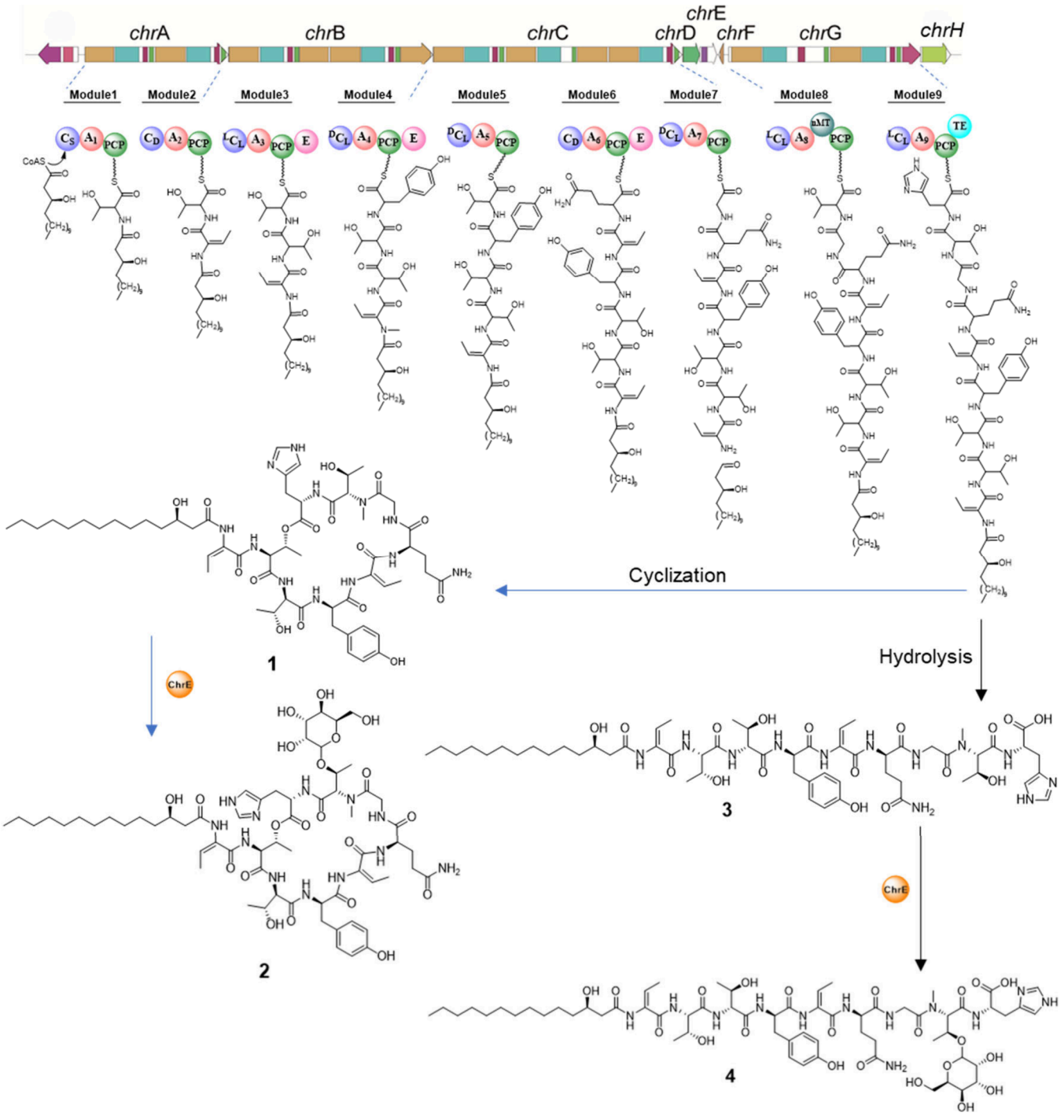

Figure 5. Proposed biosynthetic pathway of chromorhipeptins. A, adenylation domain; C, condensation domain; $^{L}C_{L}$, condensation for two L-amino acids; $^{D}C_{L}$, condensation of D-amino acid with L-amino acid; C_{D}, condensation and dehydration domain; C_{S}, starter condensation domain; E, epimerization domain; PCP, peptidyl carrier protein; and TE, thioesterase domain.

analysis method might be applicable for its configuration determination.[62,63] Based on bioinformatic analysis[64] the absence of designated epimerization domains of module 8, it is speculated to be *N*Me-L-Thr[8] or *N*Me-L-*allo*-Thr[8]. According to the *J*-based configuration analysis protocol, the large $^{3}J_{H,H}$ value (8.9 Hz) observed between the α- and β-H of *N*MeThr[8] (Table S4) indicated an H/H-*anti* orientation[62] (Figure 4B). Although the two possible stereoisomers, (2*S*,3*R*)-*N*MeThr and (2*S*,3*S*)-*N*MeThr, cannot be differentiated by analyzing the $^{2,3}J_{C/H}$ values, a NOESY correlation between the N−CH_3 and the γ-CH_3 of *N*-MeThr[8] was observed, while the correlation between the N−H of His[9] and the γ-CH_3 of *N*-MeThr[8] was absent, thus supporting a 2*S*,3*S* configuration (Figure 4C). Based on these analyses, the *N*MeThr[8] in **1** was tentatively assigned as *N*-Me-L-*allo*-Thr. Structural comparison revealed that the macrocyclic lipodepsipeptide **1** is quite similar to the jagaricin, a highly antifungal lipopeptide isolated from *Janthinobacterium agaricidamnosum* belonging to the order *Burkholderiales*.[65] Comparison of the NMR spectroscopic data of **1** with jagaricin (Table S9) revealed that they

https://doi.org/10.1021/acs.jafc.5c04892
J. Agric. Food Chem. XXXX, XXX, XXX−XXX

were highly conserved scaffold except that the signals corresponding to the L-*allo*-Thr in jagaricin were replaced by *N*-Me-L-*allo*-Thr8 in **1**, according with the molecular weight of **1** being 14 Da more than that of jagaricin.

The mass of compound **2** (m/z 1357.6815 $[M + H]^+$) is 162 Da larger than that of compound **1** (Figure S6). The signals of sugar residues corresponding to a hexose mass of 162 Da were assigned to glucosyl moieties based on the results of 1D and 2D NMR experiments (Figures S7−S19). The anomeric proton signals were found at δ_H 4.67 ($J_{H1, H2}$ = 3.5 Hz), and the corresponding ^{13}C signals were found at δ_C 97.8, according to the HSQC spectrum. The chemical shifts and coupling constants confirmed an α anomeric configuration, which were confirmed to be α-D-glucose.[66] The proton (δ_H 4.68) attached to the anomeric carbon of the α-D-glucose showed a correlation to the C_β (δ_C 61.4) of *N*Me-Thr^8 in the HMBC, thus confirming that the link of the α-D-glucose was attached to the OH of *N*Me-L-*allo*-Thr^8 (Figure 4A). The masses of **3** and **4** have an additional 18 Da compared with that of **1** and **2** (Figure S6) and they were confirmed to be the linear congeners of **1** and **2** according to NMR experiments, respectively (Figures S20−S31).

Proposed Biosynthetic Pathway for Chromorhipeptins. The structures of chromorhipeptins align well with the bioinformatic prediction based on the biosynthetic enzymes in the *chr* BGC (Figure 5). The peptidyl backbone of chromorhipeptin is biosynthesized by the cooperation of four NRPSs, ChrA, ChrB, ChrC, and ChrG. The biosynthesis begins with the recognition of β-hydroxymyristoyl-CoA by the Cs domain of ChrA. Subsequently, nine NRPS modules sequentially activate and condense the corresponding nine amino acids to assemble peptidyl chains of compounds **1**−**4** (Figure 5). The C domains in modules 2 and 6 belong to the C_D subfamily,[67] which can catalyze the dehydration of Thr^1/Thr^5 to yield Dhb^1/Dhb^5, respectively. The *N*-MT domain of ChrG is responsible for the *N*-methyl of the Thr^8 residue. The E domains in modules 3, 4, and 6 are in charge of the stereochemical inversion of Thr^3, Tyr^4, and Gln^6. The full peptidyl chain may be released from the NRPS via the TE domain, which catalyzed the cyclization between the hydroxyl group of Thr^2 and the carbonyl group of His^9 to form cyclic **1** or hydrolyzed to obtain linear **3**. This situation with simultaneous cyclic and linear lipopeptides is not unique, and presents in the gramibactins and megapolibactins.[68] Subsequently, compounds **1** and **3** may undergo glycosylation at the hydroxyl group of *N*-methyl-Thr^8 by the ChrE, yielding glycosylated derivatives **2** and **4**, respectively. The gene inactivation experiment of *chrE* led to the absence of **1**−**4** (Figure S32), suggesting that the ChrE mediates the glycosylation in the biosynthetic pathway. However, the timing of glycosylation whether occurs during peptide chain elongation or postassembly remains to be investigated in the future. The *chrD* mutant shows an identical metabolic profile to the WT (Figure S32), verifying that ChrD fails to participate in the biosynthesis of chromorhipeptins as proposed (Figure 5).

Antifungal Evaluation of Chromorhipeptins. Motivated by the structural resemblance between chromorhipeptins and the potent antifungal lipopeptide jagaricin,[67] we conducted preliminary antifungal screening against the phytopathogens and two human pathogenic fungi to evaluate their antifungal potential (Table S10). Through preliminary screening, compounds **1** and **2** demonstrated promising antifungal activity. Therefore, subsequent dose−response assays using a 2-fold liquid dilution series revealed potent and selective antifungal activities of both compounds **1** and **2** (Table 1).

Table 1. Activities of Compounds 1 and 2 against Plant Pathogenic Fungi

	MIC (μM)			
plant pathogenic fungi	**1**	**2**	carbendazim	amphotericin B
Fusarium graminearum	1.56	0.78	6.25	>50.00
Fusarium oxysporum	50.00	25.00	1.56	>50.00
Alternaria panax	50.00	50.00	6.25	>50.00
Valsa mali	0.04	0.16	0.78	>50.00
Phytophthora infestans	6.25	3.13	6.25	>50.00
Sclerotinia sclerotiorum	0.39	0.20	0.39	>50.00
Phytophthora nicotianae	>50.00	0.20	>50.00	0.39
Bipolaris sorokiniana	>50.00	50.00	3.13	>50.00
Botrytis cinerea	3.13	0.20	>50.00	0.78

Compound **1** exhibited exceptional efficacy against *Valsa mali* (MIC = 0.04 μM) and *Sclerotinia sclerotiorum* (MIC = 0.39 μM), outperforming the conventional fungicide carbendazim (MIC = 0.78 and 0.39 μM, respectively). Compound **2** demonstrated broader activity with superior inhibition against *Fusarium graminearum* (MIC = 0.78 μM) and *Botrytis cinerea* (MIC = 0.20 μM). Compounds **1** and **2** retained moderate antioomycete activity against *Phytophthora infestans* (MIC = 3.13−6.25 μM), but they failed to show activity against *Fusarium oxysporum* and *Alternaria panax* (MICs ≥ 25 μM). These results underscore the potent but specific antifungal activity of chromorhipeptins A and B and highlight their potential for targeted crop disease management.

DISCUSSION

In this study, we systematically applied genome mining to investigate the diversity and novelty of BGCs across 136 genomes in the *Chromobacterium* genus, uncovering its largely unexplored (>90%) secondary metabolite potential. Notably, 45.4% of the identified NRPS BGCs harbor a Cs domain, whereas only two exhibit known products, underscoring the promise of the genus as a source of novel lipopeptides. Among these, BGCs within GCF9 were found to contain nine NRPS modules and a gene encoding a glycosyltransferase, suggesting its potential to biosynthesize structurally unique glycolipopeptides. Through a combination of gene knockout validation and mass spectrometry, we successfully characterized the products of one BGC within GCF9, chromorhipeptins A and B, which demonstrated potent antifungal activity. Thus, our findings provide new insights into the hidden biosynthetic capacity of *Chromobacterium* spp. and also establish a targeted framework for mining microbial genomes for lipopeptide discovery, offering valuable leads for the development of antifungal agents.

Plant pathogenic fungi represent a major threat to global agricultural productivity, causing severe yield and quality losses annually.[69] Despite the widespread use of synthetic fungicides, the escalating challenge of antifungal resistance has driven the exploration of microbial secondary metabolites as a reservoir of novel antifungal agents.[37] NRLPs are well documented for their broad-spectrum antifungal properties, offering a promising strategy to circumvent conventional drug resistance. Herein, four lipopeptides, chromorhipeptins A-D, were

https://doi.org/10.1021/acs.jafc.5c04892
J. Agric. Food Chem. XXXX, XXX, XXX−XXX

successfully characterized via targeted inactivation of the *chr* gene cluster in *C. rhizoryzae* combined with compound purification and structural elucidation. Bioactivity assays revealed that chromorhipeptins A and B displayed remarkable inhibitory activity against phytopathogens, such as *Botrytis cinerea* and *Fusarium graminearum*, highlighting their broad applicability in protecting crops such as apples, grapes, and wheat. Their structural divergence from classical NRLPs (surfactins, iturins) might suggest a different mode of action that can evade existing resistance pathways. Future studies should focus on elucidating their molecular targets and evaluating field stability and ecotoxicological profiles to facilitate their development as potential agricultural antifungal agents.

■ ASSOCIATED CONTENT

Data Availability Statement

The data underlying this study are available in the published article and its Supporting Information.

Supporting Information

The Supporting Information is available free of charge at https://pubs.acs.org/doi/10.1021/acs.jafc.5c04892.

Chromobacterium genome dataset (XLSX)

Information about 1,713 BGCs identified in 136 Chromobacterium strains and eight closely related gene clusters grouped into 190 GCFs (XLSX)

NMR data, NMR spectra, MS/MS spectra, LC-MS chromatogram, strains, plasmids, and primers used in this work and other supporting figures and data (PDF)

■ AUTHOR INFORMATION

Corresponding Authors

Bin Wei − *College of Pharmaceutical Science & Collaborative Innovation Center of Yangtze River Delta Region Green Pharmaceuticals, Zhejiang Key Laboratory of Green, Low-Carbon, and Efficient Development of Marine Fishery Resources, Zhejiang University of Technology, Hangzhou 310014, China;* orcid.org/0000-0001-7362-1228; Email: binwei@zjut.edu.cn

Xiaoying Bian − *Helmholtz International Lab for Anti-Infectives, State Key Laboratory of Microbial Technology, Shandong University, Qingdao, Shandong 266237, China;* orcid.org/0000-0002-1356-3211; Email: bianxiaoying@sdu.edu.cn

Authors

Qinghong Meng − *Helmholtz International Lab for Anti-Infectives, State Key Laboratory of Microbial Technology, Shandong University, Qingdao, Shandong 266237, China*

Yutian Guan − *College of Pharmaceutical Science & Collaborative Innovation Center of Yangtze River Delta Region Green Pharmaceuticals, Zhejiang Key Laboratory of Green, Low-Carbon, and Efficient Development of Marine Fishery Resources, Zhejiang University of Technology, Hangzhou 310014, China*

Jinghai Wang − *Helmholtz International Lab for Anti-Infectives, State Key Laboratory of Microbial Technology, Shandong University, Qingdao, Shandong 266237, China*

Xingyan Wang − *Helmholtz International Lab for Anti-Infectives, State Key Laboratory of Microbial Technology, Shandong University, Qingdao, Shandong 266237, China*

Xiangmei Ren − *Helmholtz International Lab for Anti-Infectives, State Key Laboratory of Microbial Technology, Shandong University, Qingdao, Shandong 266237, China*

Haiyan Sui − *Helmholtz International Lab for Anti-Infectives, State Key Laboratory of Microbial Technology, Shandong University, Qingdao, Shandong 266237, China*

Complete contact information is available at: https://pubs.acs.org/10.1021/acs.jafc.5c04892

Notes

The authors declare no competing financial interest.

■ ACKNOWLEDGMENTS

We are grateful to Prof. Yinhua Lu from Shanghai Normal University for providing the pKCcas9dO plasmid. We would like to thank Guannan Lin from State Key Laboratory of Microbial Technology of Shandong University for HRESIMS measurements. This work was supported by the National Natural Science Foundation of China (32371488), the Fundamental Research Funds of Shandong University (2023QNTD001), the National Key R&D Program of China (2022YFC2804700), the Shandong Provisional Key R&D Program (2022CXGC020709), the Shandong Provincial Natural Science Foundation (ZR2023ZD29), the Qingdao Postdoctoral Program (QDBSH20240201014), the Intramural Joint Program Fund of State Key Laboratory of Microbial Technology (SKLMTIJP-2024-04), the SKLMT Frontiers and Challenges Project (SKLMTFCP-2023-05), and the State Key Laboratory of Microbial Technology Open Projects Fund (Project M2024-05).

■ REFERENCES

(1) Hemmerling, F.; Piel, J. Strategies to access biosynthetic novelty in bacterial genomes for drug discovery. *Nat. Rev. Drug. Discovery* **2022**, *21* (5), 359−378.

(2) Yan, Y.; Liu, Q. K.; Jacobsen, S. E.; Tang, Y. The impact and prospect of natural product discovery in agriculture: New technologies to explore the diversity of secondary metabolites in plants and microorganisms for applications in agriculture. *EMBO Rep.* **2018**, *19*, No. e46824.

(3) Li, L. Next-generation synthetic biology approaches for the accelerated discovery of microbial natural products. *Eng. Microbiol* **2023**, *3* (1), 100060.

(4) Kenshole, E.; Herisse, M.; Michael, M.; Pidot, S. J. Natural product discovery through microbial genome mining. *Curr. Opin. Chem. Biol.* **2021**, *60*, 47−54.

(5) Gavriilidou, A.; Kautsar, S. A.; Zaburannyi, N.; Krug, D.; Müller, R.; Medema, M. H.; Ziemert, N. Compendium of specialized metabolite biosynthetic diversity encoded in bacterial genomes. *Nat. Microbiol.* **2022**, *7* (5), 726−735.

(6) Wang, M. P.; Chen, L.; Zhang, Z. J.; Wang, Q. H. Recent advances in genome mining and synthetic biology for discovery and biosynthesis of natural products. *Crit. Rev. Biotechnol.* **2025**, *45* (1), 236−256.

(7) Shi, Y. M.; Hirschmann, M.; Shi, Y. N.; Ahmed, S.; Abebew, D.; Tobias, N. J.; Grün, P.; Crames, J. J.; Pöschel, L.; Kuttenlochner, W.; et al. Global analysis of biosynthetic gene clusters reveals conserved and unique natural products in entomopathogenic nematode-symbiotic bacteria. *Nat. Chem.* **2022**, *14* (6), 701−712.

(8) Deng, Q.; Li, Y.; He, W.; Chen, T.; Liu, N.; Ma, L.; Qiu, Z.; Shang, Z.; Wang, Z. A polyene macrolide targeting phospholipids in the fungal cell membrane. *Nature* **2025**, *640* (8059), 743−751.

(9) Liu, X. Y.; Currens, G. C.; Xue, L.; Cheng, Y. Q. Origin and bioactivities of thiosulfinated FK228. *Medchemcomm.* **2019**, *10* (4), 538−542.

(10) Fujioka, M.; Koda, S.; Morimoto, Y.; Biemann, K. Structure of FR900359, a cyclic depsipeptide from Ardisia crenata sims. *J. Org. Chem.* **1988**, *53* (12), 2820−2825.
(11) Chauhan, A.; Mathkor, D. M.; Joshi, H.; Chauhan, R.; Sharma, U.; Sharma, V.; Kumar, M.; Saini, R. V.; Saini, A. K.; Tuli, H. S.; et al. Mechanistic Insight of Pharmacological Aspects of Violacein: Recent Trends and Advancements. *J. Biochem Mol. Toxic.* **2025**, *39* (2), No. e70114.
(12) Parker, W. L.; Koster, W. H.; Cimarusti, C. M.; Floyd, D. M.; Liu, W.-C.; Rathnum, M. SQ 26, 180, a novel monobactam. II Isolation, structure determination and synthesis. *J. Antiobiot.* **1982**, *35* (2), 189−195.
(13) Parker, W. L.; Rathnum, M. L.; Johnson, J. H.; Wells, J. S.; Principe, P. A.; Sykes, R. B. Aerocyanidin, a New Antibiotic Produced by *Chromobacterium violaceum*. *J. Antibiot.* **1988**, *41* (4), 454−460.
(14) Jiang, P. X.; Wang, H. S.; Xiao, S.; Fang, M. Y.; Zhang, R. P.; He, S. Y.; Lou, K.; Xing, X.-H. Pathway redesign for deoxyviolacein biosynthesis in Citrobacter freundii and characterization of this pigment. *Appl. Microbiol. Biotechnol.* **2012**, *94*, 1521−1532.
(15) Richard, C. Chromobacterium violaceum, opportunist pathogenic bacteria in tropical and subtropical regions. *Bull. Soc. Pathol Exot.* **1993**, *86* (3), 169−173.
(16) Hugon, P.; Lagier, J. C.; Colson, P.; Bittar, F.; Raoult, D. Repertoire of human gut microbes. *Microb. Pathogenesis.* **2017**, *106*, 103−112.
(17) Shannag, H. K.; Al-Salman, A. A. Lethal and sublethal effects of selected bacterial and neem-based novel insecticides on cotton aphid, and the predator. *Bull. Entomol. Res.* **2025**, *115*, 141−154.
(18) Pistorius, D.; Buntin, K.; Richard, E.; Rust, M.; Bouquet, C.; Wollbrett, S.; Weber, E.; Dietschin, D.; Bruccoleri, R.; Oakeley, E.; et al. Valhidepsin lipopeptides from Chromobacterium vaccinii: structures, biosynthesis, and coregulation with FR900359 production. *J. Nat. Prod.* **2023**, *86* (2), 246−255.
(19) Liu, W. X.; Ji, X. Q.; Bian, X. Y. Research progress on natural products and their biosynthesis from Chromobacterium spp. *Chin. J. Antibiot* **2025**, *50* (5), 508−522.
(20) Kautsar, S. A.; Blin, K.; Shaw, S.; Weber, T.; Medema, M. H. BiG-FAM: the biosynthetic gene cluster families database. *Nucleic. Acids. Res.* **2021**, *49* (D1), D490−D497.
(21) Schwarzer, D.; Finking, R.; Marahiel, M. A. Nonribosomal peptides: from genes to products. *Nat. Prod. Rep.* **2003**, *20* (3), 275−287.
(22) Fischbach, M. A.; Walsh, C. T. Assembly-line enzymology for polyketide and nonribosomal peptide antibiotics: logic, machinery, and mechanisms. *Chem. Rev.* **2006**, *106* (8), 3468−3496.
(23) Marahiel, M. A.; Stachelhaus, T.; Mootz, H. D. Modular peptide synthetases involved in nonribosomal peptide synthesis. *Chem. Rev.* **1997**, *97* (7), 2651−2673.
(24) Challis, G. L.; Ravel, J.; Townsend, C. A. Predictive, structure-based model of amino acid recognition by nonribosomal peptide synthetase adenylation domains. *Chem. Biol.* **2000**, *7* (3), 211−224.
(25) Röttig, M.; Medema, M. H.; Blin, K.; Weber, T.; Rausch, C.; Kohlbacher, O. NRPSpredictor2-a web server for predicting NRPS adenylation domain specificity. *Nucleic. Acids. Res.* **2011**, *39* (suppl_2), W362−W367.
(26) Bednarska, N. G.; Wren, B. W.; Willcocks, S. J. The importance of the glycosylation of antimicrobial peptides: natural and synthetic approaches. *Drug. Discovery Today.* **2017**, *22* (6), 919−926.
(27) Bellavita, R.; Braccia, S.; Galdiero, S.; Falanga, A. Glycosylation and Lipidation Strategies: Approaches for Improving Antimicrobial Peptide Efficacy. *Pharmaceuticals* **2023**, *16* (3), 439.
(28) Chen, H.; Zhong, L.; Zhou, H. B.; Bai, X. P.; Sun, T.; Wang, X. Y.; Zhao, Y. M.; Ji, X. Q.; Tu, Q.; Zhang, Y. M.; et al. Biosynthesis and engineering of the nonribosomal peptides with a C-terminal putrescine. *Nat. Commun.* **2023**, *14* (1), 6619.
(29) Chen, H. N.; Sun, T.; Bai, X. P.; Yang, J.; Yan, F.; Yu, L.; Tu, Q.; Li, A. Y.; Tang, Y. J.; Zhang, Y. M.; et al. Genomics-Driven Activation of Silent Biosynthetic Gene Clusters in by Screening Recombineering System. *Molecules* **2021**, *26* (3), 700.
(30) Zhong, L.; Diao, X. T.; Zhang, N.; Li, F. W.; Zhou, H. B.; Chen, H. N.; Bai, X. P.; Ren, X. T.; Zhang, Y. M.; Wu, D. L.; et al. Engineering and elucidation of the lipoinitiation process in nonribosomal peptide biosynthesis. *Nat. Commun.* **2021**, *12* (1), 296.
(31) Niu, W. J.; Liu, J. Q.; Duan, Y. W.; Zhong, L.; Pang, L. L.; Zhong, G. N.; Zhang, Y. M.; Bian, X. Y. Biosynthesis of Nonribosomal Peptides Chitinimides Reveal a Special Type of Thioesterase Domains. *Chem.—Eur. J.* **2024**, *30* (69), No. e202402763.
(32) Sani, A.; Qin, W. Q.; Li, J. Y.; Liu, Y. F.; Zhou, L.; Yang, S. Z.; Mu, B. Z. Structural diversity and applications of lipopeptide biosurfactants as biocontrol agents against phytopathogens: A review. *Microbiol. Res.* **2024**, *278*, 127518.
(33) Chauhan, V.; Mazumdar, S.; Pandey, A.; Kanwar, S. S. Pseudomonas lipopeptide: An excellent biomedical agent. *MedComm-Biomaterials and Applications* **2023**, *2* (1), No. e27.
(34) Götze, S.; Stallforth, P. Structure, properties, and biological functions of nonribosomal lipopeptides from pseudomonads. *Nat. Prod. Rep.* **2020**, *37* (1), 29−54.
(35) Bellavita, R.; Braccia, S.; Galdiero, S.; Falanga, A. Glycosylation and Lipidation Strategies: Approaches for Improving Antimicrobial Peptide Efficacy. *Pharmaceuticals* **2023**, *16* (3), 439.
(36) Hansanant, N.; Smith, L. Occidiofungin: Actin Binding as a Novel Mechanism of Action in an Antifungal Agent. *Antibiotics-Basel* **2022**, *11* (9), 1143.
(37) Humisto, A.; Jokela, J.; Teigen, K.; Wahlsten, M.; Permi, P.; Sivonen, K.; Herfindal, L. Characterization of the interaction of the antifungal and cytotoxic cyclic glycolipopeptide hassallidin with sterol-containing lipid membranes. *BBA-Biomembranes* **2019**, *1861* (8), 1510−1521.
(38) Wick, R. R.; Judd, L. M.; Gorrie, C. L.; Holt, K. E. Unicycler: Resolving bacterial genome assemblies from short and long sequencing reads. *Plos. Comput. Biol.* **2017**, *13* (6), No. e1005595.
(39) Sayers, E. W.; Beck, J.; Bolton, E. E.; Brister, J. R.; Chan, J.; Connor, R.; Feldgarden, M.; Fine, A. M.; Funk, K.; Hoffman, J.; et al. Database resources of the National Center for Biotechnology Information in 2025. *Nucleic. Acids. Res.* **2025**, *53* (D1), D20−D29.
(40) Chklovski, A.; Parks, D. H.; Woodcroft, B. J.; Tyson, G. W. CheckM2: a rapid, scalable and accurate tool for assessing microbial genome quality using machine learning. *Nat. Methods.* **2023**, *20* (8), 1203−1212.
(41) Na, S. I.; Kim, Y. O.; Yoon, S. H.; Ha, S. M.; Baek, I.; Chun, J. UBCG: Up-to-date bacterial core gene set and pipeline for phylogenomic tree reconstruction. *J. Microbiol.* **2018**, *56* (4), 280−285.
(42) Letunic, I.; Bork, P. Interactive Tree Of Life (iTOL) v5: an online tool for phylogenetic tree display and annotation. *Nucleic. Acids. Res.* **2021**, *49* (W1), W293−W296.
(43) Blin, K.; Shaw, S.; Kloosterman, A. M.; Charlop-Powers, Z.; van Wezel, G. P.; Medema, M. H.; Weber, T. antiSMASH 6.0: improving cluster detection and comparison capabilities. *Nucleic. Acids. Res.* **2021**, *49* (W1), W29−W35.
(44) Zdouc, M. M.; Blin, K.; Louwen, N. L. L.; Navarro, J.; Loureiro, C.; Bader, C. D.; Bailey; Constance, B.; Barra, L.; Booth, T. J.; Bozhüyük, K. A. J.; et al. MIBiG 4.0: advancing biosynthetic gene cluster curation through global collaboration. *Nucleic. Acids. Res.* **2025**, *53* (D1), D678−D690.
(45) Navarro-Muñoz, J. C.; Selem-Mojica, N.; Mullowney, M. W.; Kautsar, S. A.; Tryon, J. H.; Parkinson, E.; De Los Santos, E. L. C.; Yeong, M.; Cruz-Morales, P.; Abubucker, S.; et al. A computational framework to explore large-scale biosynthetic diversity. *Nat. Chem. Biol.* **2020**, *16* (1), 60−68.
(46) Shannon, P.; Markiel, A.; Ozier, O.; Baliga, N. S.; Wang, J. T.; Ramage, D.; Amin, N.; Schwikowski, B.; Ideker, T. Cytoscape: A software environment for integrated models of biomolecular interaction networks. *Genome. Res.* **2003**, *13* (11), 2498−2504.
(47) Van den Belt, M.; Gilchrist, C.; Booth, T. J.; Chooi, Y. H.; Medema, M. H.; Alanjary, M. CAGECAT: The CompArative GEne Cluster Analysis Toolbox for rapid search and visualisation of homologous gene clusters. *BMC Bioinformatics* **2023**, *24* (1), 181.

https://doi.org/10.1021/acs.jafc.5c04892
J. Agric. Food Chem. XXXX, XXX, XXX−XXX

(48) Price, M. N.; Dehal, P. S.; Arkin, A. P. FastTree: Computing Large Minimum Evolution Trees with Profiles instead of a Distance Matrix. *Mol. Biol. Evol.* **2009**, *26* (7), 1641−1650.
(49) Wang, X. Y.; Zhou, H. B.; Ren, X. M.; Chen, H. N.; Zhong, L.; Bai, X. P.; Bian, X. Y. Recombineering enables genome mining of novel siderophores in a non-model Burkholderiales strain. *Eng. Microbiol.* **2023**, *3* (3), 100106.
(50) Khajanchi, B. K.; Kaldhone, P. R.; Foley, S. L. Protocols of conjugative plasmid transfer in *Salmonella*: plate, broth, and filter mating approaches. In *Microbial Transposon Mutagenesis: Protocols and Applications*; Williams, S. M.; Barabote, R. D.; Fouts, D. E., Eds.; Methods in Molecular Biology, Vol. *2016*; Humana Press: New York, NY, 2019; pp 129−139.
(51) Wei, J.; Li, Y. CRISPR-based gene editing technology and its application in microbial engineering. *Eng. Microbiol.* **2023**, *3* (4), 100101.
(52) Huang, H.; Zheng, G.; Jiang, W.; Hu, H.; Lu, Y. One-step high-efficiency CRISPR/Cas9-mediated genome editing in Streptomyces. *Acta. Bioch. Bioph. Sin.* **2015**, *47* (4), 231−243.
(53) Fujii, K.; Ikai, Y.; Oka, H.; Suzuki, M.; Harada, K. A nonempirical method using LC/MS for determination of the absolute configuration of constituent amino acids in a peptide: Combination of Marfey's method with mass spectrometry and its practical application. *Anal. Chem.* **1997**, *69* (24), 5146−5151.
(54) Trzcinska-Wencel, J.; Wypij, M.; Rai, M.; Golinska, P. Biogenic nanosilver bearing antimicrobial and antibiofilm activities and its potential for application in agriculture and industry. *Front. Microbiol.* **2023**, *14*, 1125685.
(55) Balibar, C. J.; Walsh, C. T. In vitro biosynthesis of violacein from L-tryptophan by the enzymes VioA-E from. *Biochemistry-Us* **2006**, *45* (51), 15444−15457.
(56) Wesener, S. R.; Potharla, V. Y.; Cheng, Y. Q. Reconstitution of the FK228 Biosynthetic Pathway Reveals Cross Talk between Modular Polyketide Synthases and Fatty Acid Synthase. *Appl. Environ. Microb.* **2011**, *77* (4), 1501−1507.
(57) Zheng, Z. Y.; Clardy, J.; Liu, H. W. Biosynthesis of the Unusual Epoxy Isonitrile-Containing Antibiotics Aerocyanidin and Amycomicin. *J. Am. Chem. Soc.* **2024**, *146* (30), 21061−21068.
(58) Batista, B. B.; Santos, R. E. R. d. S.; Ricci-Azevedo, R.; da Silva Neto, J. F. Production and Uptake of Distinct Endogenous Catecholate-Type Siderophores Are Required for Iron Acquisition and Virulence in *Chromobacterium violaceum*. *Infect. Immun.* **2019**, *87* (12), 1110−1128.
(59) Crüsemann, M.; Reher, R.; Schamari, I.; Brachmann, A. O.; Ohbayashi, T.; Kuschak, M.; Malfacini, D.; Seidinger, A.; Pinto-Carbó, M.; Richarz, R.; et al. Heterologous Expression, Biosynthetic Studies, and Ecological Function of the Selective Gq-Signaling Inhibitor FR900359. *Angew. Chem., Int. Ed.* **2018**, *57* (3), 836−840.
(60) Dekimpe, S.; Masschelein, J. Beyond peptide bond formation: the versatile role of condensation domains in natural product biosynthesis. *Nat. Prod. Rep.* **2021**, *38* (10), 1910−1937.
(61) Neuhof, T.; Schmieder, P.; Preussel, K.; Dieckmann, R.; Pham, H.; Bartl, F.; Von Döhren, H. Hassallidin A, a glycosylated lipopeptide with antifungal activity from the cyanobacterium Hassallia sp. *J. Nat. Prod.* **2005**, *68* (5), 695−700.
(62) Matsumori, N.; Kaneno, D.; Murata, M.; Nakamura, H.; Tachibana, K. Stereochemical determination of acyclic structures based on carbon- proton spin-coupling constants. A method of configuration analysis for natural products. *J. Org. Chem.* **1999**, *64* (3), 866−876.
(63) Xiao, D. L.; Li, W. H.; Li, T. Y.; Zhou, J. S.; Zhang, M.; Chen, X. Q.; Zhang, L. W.; Yue, Q.; Dun, B. Q.; Wang, C.; Xu, Y. Q. Mass spectrometry-guided discovery of multi-n-methylated cyclodecapeptides auyuittuqamides E-H from Sesquicillium sp. QL0466. *J. Nat. Prod.* **2023**, *86* (5), 1240−1250.
(64) Thongkongkaew, T.; Ding, W.; Bratovanov, E.; Oueis, E.; Garcıa-Altares, M.; Zaburannyi, N.; Harmrolfs, K.; Zhang, Y.; Scherlach, K.; Muller, R.; Hertweck, C. Two types of threonine-tagged lipopeptides synergize in host colonization by pathogenic Burkholderia species. *ACS Chem. Biol.* **2018**, *13* (5), 1370−1379.
(65) Graupner, K.; Scherlach, K.; Bretschneider, T.; Lackner, G.; Roth, M.; Gross, H.; Hertweck, C. Imaging Mass Spectrometry and Genome Mining Reveal Highly Antifungal Virulence Factor of Mushroom Soft Rot Pathogen. *Angew. Chem. Int. Ed.* **2012**, *51* (52), 13173−13177.
(66) Bubb, W. A. NMR spectroscopy in the study of carbohydrates: Characterizing the structural complexity. *Concept. Magn. Reson. A* **2003**, *19a* (1), 1−19.
(67) Patteson, J. B.; Fortinez, C. M.; Putz, A. T.; Rodriguez-Rivas, J.; Bryant, L.; Adhikari, K.; Weigt, M.; Schmeing, T. M.; Li, B. Structure and Function of a Dehydrating Condensation Domain in Non-ribosomal Peptide Biosynthesis. *J. Am. Chem. Soc.* **2022**, *144* (31), 14057−14070.
(68) Hermenau, R.; Mehl, J. L.; Ishida, K.; Dose, B.; Pidot, S. J.; Stinear, T. P.; Hertweck, C. Genomics-driven discovery of NO-Donating Diazeniumdiolate Siderophores in diverse plant-associated bacteria. *Angew. Chem. Int. Ed.* **2019**, *58* (37), 13024−13029.
(69) Savary, S.; Ficke, A.; Aubertot, J. N.; Hollier, C. Crop losses due to diseases and their implications for global food production losses and food security. *Food. Secur.* **2012**, *4* (4), 519−537.

https://doi.org/10.1021/acs.jafc.5c04892
J. Agric. Food Chem. XXXX, XXX, XXX−XXX